Elastic Deformation of Soft Coatings Due to Lubrication Forces

Yumo Wang, Matthew R. Tan, and Joelle Frechette*
Chemical and Biomolecular Engineering and Hopkins Extreme Materials Institute, Johns Hopkins University, Baltimore, MD 21218

Supporting Information

1. Non-dimensionalization of the governing equations

We non-dimensionalize our systems of equations (Equations 1-5). Naturally, the characteristic separation should be initial separation, so that the dimensionless separation is $\hat{h} = \frac{h}{h_0}$, and $\hat{h}$ start at 1 during experiments and the contact position is at $\hat{h} = 0$. We set the dimensionless radial position to be $\hat{r} = \frac{r}{r_0} = \frac{r}{\sqrt{Rh_0}}$, normalize *r* by the initial hydrodynamic radius. If we substitute *h* and *r* in Equation 1 with their dimensionless variables and rearrange we get:

$$\frac{h_0}{t_0}\frac{\partial \hat{h}}{\partial \hat{t}} = \frac{1}{12\eta \hat{r}} \cdot \frac{1}{\sqrt{Rh_0}} \cdot \frac{{h_0}^3 p_0}{\sqrt{Rh_0}} \frac{\partial}{\partial \hat{r}}\left(\hat{r}\hat{h}^3 \frac{\partial \hat{p}}{\partial \hat{r}}\right).$$

Note that t_0 and p_0 are assumed dimensionless parameters for time and pressure. From Equation 5, we know that Vt and w should have the dimensionless parameter of h_0 (same as h), because they are being added or subtracted from h. Therefore, $t_0 = \frac{t}{\hat{t}} = \frac{h_0}{V}$. After re-arranging and cancelling terms, we have:

$$\frac{\partial \hat{h}}{\partial \hat{t}} = \frac{1}{12\hat{r}} \cdot \frac{{h_0}^2 p_0}{\eta RV} \frac{\partial}{\partial \hat{r}}\left(\hat{r}\hat{h}^3 \frac{\partial \hat{p}}{\partial \hat{r}}\right).$$

We then set p_0 to be $\frac{\eta RV}{{h_0}^2}$, then:

$$\frac{\partial \hat{h}}{\partial \hat{t}} = \frac{1}{12\hat{r}} \cdot \frac{\partial}{\partial \hat{r}}\left(\hat{r}\hat{h}^3 \frac{\partial \hat{p}}{\partial \hat{r}}\right)$$

Which is the Equation 6 in the paper. If we further put dimensionless parameters acquired so far into Equation 5:

$$k(\hat{h} - 1 + \hat{t} - \hat{w}) \cdot h_0 = \int 2\pi \hat{r}\hat{p} d\hat{r} \cdot Rh_0 \frac{\eta RV}{{h_0}^2}$$

Therefore:

$$\hat{F} = = \int 2\pi \hat{r}\hat{p} d\hat{r} = \frac{k{h_0}^2}{\eta R^2 V}(\hat{h} - 1 + \hat{t} - \hat{w})$$

* To whom correspondence should be addressed: jfrechette@jhu.edu

Which is the Equation 10 in the paper if we denote spring parameter K as $\frac{kh_0^{\,2}}{\eta R^2 V}$.

In equation 4, all the dimensional parameters are known, except for Hankel transform variable ξ. However, since ξr is dimensionless, $\hat{\xi} = \xi\sqrt{Rh_0}$, and the dimensional parameters of ξr cancel out in the Bessel function. We can render Z into dimensionless term:

$$Z = \hat{\xi}\int_0^\infty \hat{r}\hat{p}J_0(\hat{\xi}\hat{r})d\hat{r}\cdot\sqrt{Rh_0}\cdot\frac{\eta RV}{h_0^{\,2}} = \hat{Z}\cdot\frac{\eta R^{1.5}V}{h_0^{\,1.5}}$$

From equation 3, we can see that the dimensional parameter for elastic coating thickness, δ, should be $\sqrt{Rh_0}$, since δ is multiplied with ξ to be the exponential order. From that, we set $T = \frac{\delta}{\sqrt{Rh_0}}$ to be the dimensionless coating thickness, which is also a key parameter.

If we then put all parameters into equation 2, after re-arrange and cancel terms, we have:

$$w = \hat{w}\cdot h_0 = \frac{\eta R^{1.5}V}{h_0^{\,1.5}}\cdot\frac{1}{E^*}\int_0^\infty \frac{2}{\hat{\xi}}X(\hat{\xi}T)\hat{Z}J_0(\hat{\xi}\hat{r})d\hat{\xi}$$

And therefore:

$$\hat{w} = \varepsilon\int_0^\infty \frac{2}{\hat{\xi}}X(\hat{\xi}T)\hat{Z}(\hat{\xi})J_0(\hat{\xi}\hat{r})d\hat{\xi},$$

with $\varepsilon = \frac{\eta R^{1.5}V}{h_0^{\,2.5}E^*}$, which is our third key dimensionless parameter.

Note that in the above analysis, the E^* and $X(\xi\delta)$ terms both have the Poisson's ratio. In the current model, we set the Poisson's ratio to be 0.5 (constant), which represents incompressible materials. If the Poisson's ratio is not set to a known numerical value, the non-linear dependence of $X(\xi\delta)$ with respect to the Poisson's ratio in equation 3 makes it hard to extract the contribution of the Poison's ratio into a dimensionless parameter. This issue has been overcome in previous works [1, 2] by expanding equation 3 for limiting cases (thin or thick films). For example, expand $X(\xi\delta)$ at $\xi\delta \sim 0$ (thin film) lead to $X(\xi\delta) \sim \xi\delta(1-2\nu)/(2(1-\nu)^2)$ for $\nu < 0.5$. Note that here the contribution of Poisson's ratio in $X(\xi\delta)$ is separated from the contribution of $\xi\delta$, and the $(1-2\nu)/(2(1-\nu)^2)$ part can be taken out from the integration in equation 2 because it's independent of ξ. By this method, the scaling of ν in ε that works for all ν could be found, but just for thin films. Since we seek a general framework that is valid for all thicknesses and elasticity, including intermediate film thicknesses, we did not expand $X(\xi\delta)$ but set the Poisson's ratio to be a constant value of 0.5, so that the choice of elasticity parameter with respect to ν won't have an effect on the numerical results. Note that for Poisson's ratio < 0.5, the dimensional numerical results using our model are still CORRECT. However, a modification parameter with respect to Poisson's ratio might be needed for comparing the dimensionless results of $\nu = 0.5$ with $\nu < 0.5$ that have the same elastic parameter.

2. *Numerical Algorithm*

2.1. Flow chart

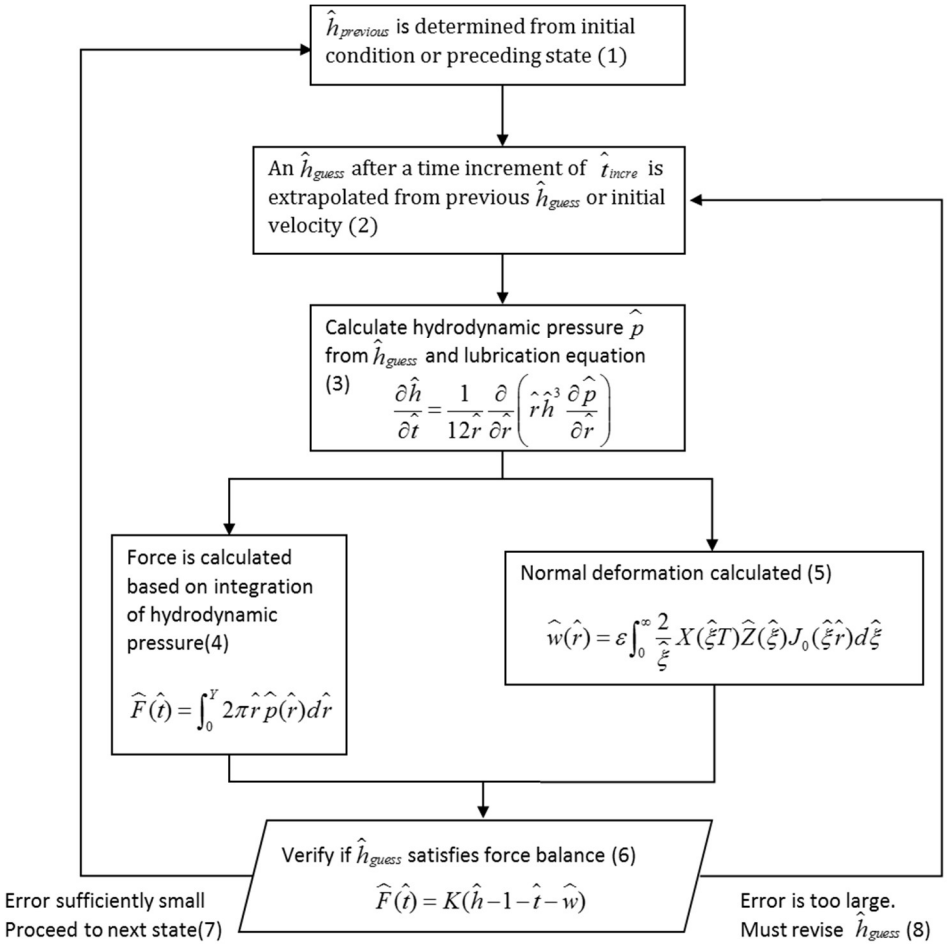

Fig. S1. Flow chart for the numerical algorithm employed.

2.2. Remarks on the flow chart.

(1) To initialize the calculation the surface at $\hat{t} = 0$ was set to be undeformed and stationary and the hydrodynamic pressure is zero.

(2) The technique of backward finite difference was used to update variables such as $d\hat{h}/d\hat{t}$.

(3) Since pressure is axially symmetric, the $\frac{\partial \hat{p}}{\partial \hat{r}}(\hat{r} = 0) = 0$. The pressure at far side $\hat{r} = 0.1\sqrt{\frac{R}{h_0}}$ ($r = 0.1R$ in dimensional form) was set to be zero and pressure was neglected for $\hat{r} > 0.1\sqrt{\frac{R}{h_0}}$. The vector $\hat{r}\hat{h}^3 \frac{\partial \hat{p}}{\partial \hat{r}}$ could be fitted using Matlab command "spline" and "fnval".

(4) The liquid pressure for $\hat{r} > 0.1\sqrt{\frac{R}{h_0}}$ is neglected. Thus, the cutoff value Y was set to be $0.1\sqrt{\frac{R}{h_0}}$.

(5) The Hankel transform variable ξ was carefully meshed (1000 points) to ensure accuracy of integration. Usually the maximum value of ξ taken was $\sim 10^5$. Note that some noise in integrant could be observed at very large ξ, if the mesh of $\hat{r}$ is not fine enough.

(6) The error in $\hat{h}_{guess}$ was transferred back into dimensional term and the tolerance criteria was set to be 0.01 nm, which is beyond the resolution of most experiments. However, a better initial $\hat{h}_{guess}$ can be gained if a smaller tolerance criteria is used, especially when the surfaces are very close.

(7) A simple method to update the new $\hat{h}_{guess}$ is to decrease the separation needed to satisfy the force balance (Step 6). ($\hat{h}^*_{guess} = 0.5(\hat{h}_{guess} + \hat{h}_{calculated})$). Here the $\hat{h}^*_{guess}$ represents the revised $\hat{h}_{guess}$ for proceeding iteration step, and $\hat{h}_{calculated}$ is the calculated separation from the force balance (Step 6) along with the hydrodynamic force from integration of pressure (Step 4). However, due to the nature of lubrication equation, at small separations, the pressure tends to be extremely sensitive to the change of separation. Therefore, a small change in $\hat{h}_{guess}$ might results in huge change in pressure, and the iteration can diverge. To improve the convergence, a weight factor (w_f) ranging from 0 to 1 is used in updating $\hat{h}_{guess}$, and the new $\hat{h}^*_{guess}$ is $w_f(\hat{h}_{guess} + (1-w_f)\hat{h}_{calculated})$. If w_f is set to be close to 1, the change $\hat{h}_{guess}$ after each iteration is relatively small and more iterations need to be run before a satisfactory solution is reached. On the other hand, because the convergence decreases with decreasing surface separations, the weight factor need to be modified to be closer to 1 over time. This trade-off limits the efficiency of computation. In the current model, w_f could be as large as 0.999 when surfaces are close.

3. Validation of layered theory

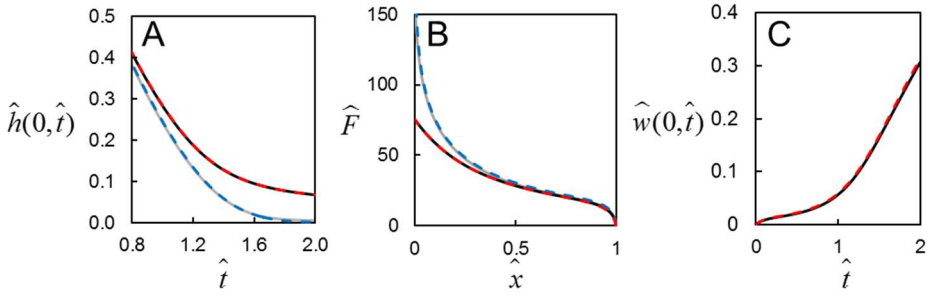

Fig. S2. Comparison of Elastohydrodynamic stratified theory with known limits: DSH model plotted in red dashed lines, and Reynolds' theory plotted in blue dashed lines. In all figures, Spring parameter K is set to be 200, and Elasticity parameter (ε) for deformable surfaces are set to be 0.0026. Grey lines: T = 0.01. Black lines: T = 20. Red dashed lines: DSH theory for half space. Blue dashed lines: Reynolds' theory for rigid surfaces.

We validate our results by recovering two well-known theories: Reynolds' theory for rigid surfaces,[3] and DSH theory for soft half-space.[4] Regardless of coating material, a surface with an extremely thin coating would have negligible deformation due to constraints of a rigid substrate. In that case, it would be adequate to describe the drainage process from Taylor equation, $F = \frac{6\pi\eta R^2}{h}\frac{dh}{dt}$. In our model, if we set the thickness parameter to very small values, for example T = 0.01, we find that our results overlap with Taylor equation (see Figure S2), in which Reynolds' theory is plotted in dashed blue lines and the layered model for T = 0.01 is plotted in grey solid lines. The overlapping between two methods is found for all the central

separation $\hat{h}(0,\hat{t})$, repulsive force $\hat{F}$ and central deformation $\hat{w}(0,\hat{t})$. On the other hand, in absence of substrate effects, drainage past a surface with an extremely thick compliant film will mimic that of a half-space. We take DSH model for elastic half-space and compare it with our model for the same elasticity but for a thickness parameter of T = 20, and find the force curves overlap again. In Figure S2, the red dashed lines indicate the DSH model and black solid lines indicate the new model with T = 20. Therefore we recover both the extremely thin and thick limits, by simply changing one parameter without different assumptions.

4. Non-monotonic relations on Force vs. separation curve for varying coating thickness

The reason for the non-monotonic dependence shown in Figure 5 is because of initialization of spring deflection in the experiments. To magnify this effect and discuss its origin, we first look at the limiting case of $K \sim \infty$, which correspond to the case of using an infinitely rigid spring compared to the compliance of surface. At the beginning of the experiments (t = 0), the motor is at rest and have a moving speed of 0, so there is no deflection, no deformation, and h is kept at h_0. After the first time increment, the motor move VΔt towards the other surface. In the limiting case where $K \sim \infty$, the displacement of the motor (point A in schematic Fig. S3(Left) will be fully transmitted to the surface (point B in schematic), and the movement of point B generates drainage flow. For rigid surfaces, because of the absence of compliant coatings, there is no deformation at this step, and $h = x$. Therefore, $V = dh/dt$ = constant, so that at the first time increment, the hydrodynamic force needs to be updated from 0 to a finite value directly ($F = \frac{6\pi\eta R^2 V}{h}$, see the "vertical wall" of rigid black line in Fig. S3(Right). For a deformable surface, however, drainage flow deforms the coating instantly and as a result the value of dh/dt is no longer equal to, but smaller than V, because the deformation increases the separation. So the initial value of the hydrodynamic force is $F = \frac{6\pi\eta R^2}{h} \cdot \frac{dh}{dt} < \frac{6\pi\eta R^2 V}{h}$. See zoom-in of Fig. S3(Right). The thicker the coating is, the larger the difference between dh/dt and V because of deformation. However, at smaller central separation, for a given h, since a more compliant surface will have a broader interacting zone with the other surface, the repulsive force tends to be larger for the softer surface. As a result, this additional effect compensates for the initiation effect

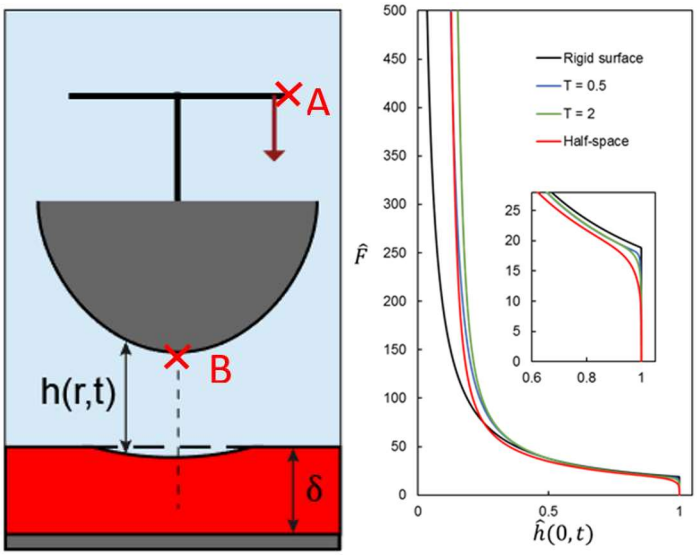

Fig. S3. (Left) Schematic illustration of spring initialization in the case of infinitely rigid spring. Red A and B: reference points indicated by red cross. $h(r,t)$ indicate the surface separation and δ is elastic coating thickness. (Right) Repulsive hydrodynamic force as a function of dimensionless surface separation for

discussed above. So, a transition and non-monotonic effects are observed in the *f* vs *h* curve for different coating thicknesses (Fig.5A and Fig. S3). As the surfaces approach, the lubrication pressure gets much bigger, and the substrate effects is getting increasingly important, and will finally dominate over the finite initiation effects. Therefore, we would ultimately see the red line on figures below going on top of other lines, if we plot Force to large enough range.

We have run the divergence test for finer time increments and concluded that this result is not due to our artifact of the numerical method. In the case of a finite spring, for example, the $K = 200$ case plotted in Figure 5A, the non-monotonic effect are much less pronounced compared to $K \sim \infty$ because the displacement of point B in schematic above now can be balanced with spring deflection, instead of directly transmitted from displacement of point A.

References

1 S. Leroy and E. Charlaix, *J. Fluid Mech.*, 2011, **674**, 389-407.
2 N. Balmforth, C. Cawthorn and R. Craster, *J. Fluid Mech.*, 2010, **646**, 339-361.
3 O. Reynolds, *Proc. R. Soc. Lond.*, 1886, **40**, 191-203.
4 R. H. Davis, J.-M. Serayssol and E. Hinch, *J. Fluid Mech.*, 1986, **163**, 479-497.